

# Mesolevel analysis of fracture tests for concrete

G. Cusatis, M. Polli & L. Cedolin

*Politecnico di Milano University, Milan, Italy.*

**ABSTRACT:** The cohesive crack model is, nowadays, widely used for the analysis of propagating cracks in concrete and other quasi-brittle materials. So far the material parameters defining this model have been considered as material properties and have been identified through the simulation of experimental tests. In this study the analysis of single notched specimens subjected to tensile loading, often used for the characterization of the fracture behavior of concrete, is analyzed on the basis of a recent meso-structural model. A procedure to obtain a macroscopic cohesive crack law from the meso-level response is outlined and the calculated macroscopic response is analyzed in order to define the actual macroscopic material properties of concrete fracture.

**Keywords:** lattice model, mesostructure, fracture energy, cohesive crack model

## 1 INTRODUCTION

The cohesive crack model is considered as the best compromise between simplicity and accuracy for the description of the fracture growth in concrete. The stress versus crack opening displacement curve, which describes the loss of carrying capacity of the two adjacent crack surfaces, is usually defined by only two parameters. One is the tensile strength,  $f_t'$ , which identifies the peak of the curve and the other is the *total fracture energy*,  $G_F$ , defining the total area under the curve (e.g. Hillerborg 1976). More recently it has been observed (Guinea et al. 1992) that only the initial part of the softening curve is relevant to the structural performance (structural peak load). This part of the softening curve can be efficiently described by the *initial fracture energy*,  $G_f$ , which represents the area under the initial tangent of the softening curve.

In the present study the macroscopic fracture energies and the macroscopic tensile strength are identified on the basis of a multiscale procedure by using a meso-structural lattice-type model recently developed (Cusatis 2001, Cusatis 2003, Cusatis et al. 2003a, b, Polli 2003) which extends previous concepts introduced by Bažant et al. (1990).

In Section 2 the formulation of the adopted model (*Confinement-Shear Lattice model*) is briefly outlined. Section 3 presents the numerical simulations of single-notched specimens subjected to tension which lead to the identification (presented in Section 4) of the parameters of the cohesive crack model.

## 2 BACKGROUND AND BRIEF REVIEW OF THE MODEL FORMULATION

In the past decades many studies have been devoted to the formulation of theories which try to simulate directly the heterogeneous character of the quasi-brittle material mesostructure. The *numerical concrete* (Roelfstra et al. 1985) is one of the first attempts in this direction. Coarse aggregates and surrounding mortar are discretized by a fine FE mesh and fracture is simulated by using interface element with cohesive behavior. Similar model have been recently proposed by López et al. (2001) and Carol et al. (2001).

This approach is often very demanding from a computational point of view and then many authors have tried to simulate the material mesostructure by replacing the continuum *a priori* by a system of

discrete elements. These models have been extensively used for simulating concrete fracture behavior in the past decades, see Bažant et al. 1990, Schlangen & van Mier 1992, Bolander & Saito 1998, Bolander et al. 2000, and Lilliu & van Mier 2003. Except for the latter, all the previous models are two-dimensional. The model of Bažant et al. (1990) differs from the others because it simulates, in a simplified fashion, the interaction between two adjacent aggregates by means of a single connection whose behavior is an average of the mechanical behavior of the aggregates and the matrix. This model can satisfactorily simulate composite mesostructure with high aggregate density (which is the case of concrete) but it is unfit to model composites with low aggregate density. On the contrary, the models of van Mier and co-workers and of Bolander and co-workers do not suffer of such a limitation since they explicitly reproduce the multiphase concrete meso-structure by using a very fine discretization and by assigning different material properties to the elements of the system. These approaches give a better representation of the meso-structure but lead to a substantial increase of the model computational cost.

The model used in the present study, which is a refinement of the model by Bažant et al. (1990), is called *Confinement-Shear Lattice model (CSL model)* and is characterized by the following features:

1. it simulates the concrete mesostructure by a three-dimensional system of interacting aggregate particles connected by a lattice which is obtained through a Delaunay triangulation of the aggregate centers;
2. the position of each aggregate piece throughout a given concrete specimen is defined by means of the basic concrete properties and the granulometric distribution of the aggregates;
3. the generic lattice element connecting two adjacent aggregate pieces transmits normal and shear stresses which are assumed to be functions of normal and shear strains;
4. the stresses are computed from the strains by a damage-like constitutive relation and by using the concept of stress-strain boundary;
5. the mesolevel constitutive behavior is softening for tension, shear-tension and shear with low compression, and, on the contrary, it is hardening for compression and shear with high compression.
6. the stresses act on a contact area which is defined by constructing a baricentric dual complex of the Delaunay triangulation;

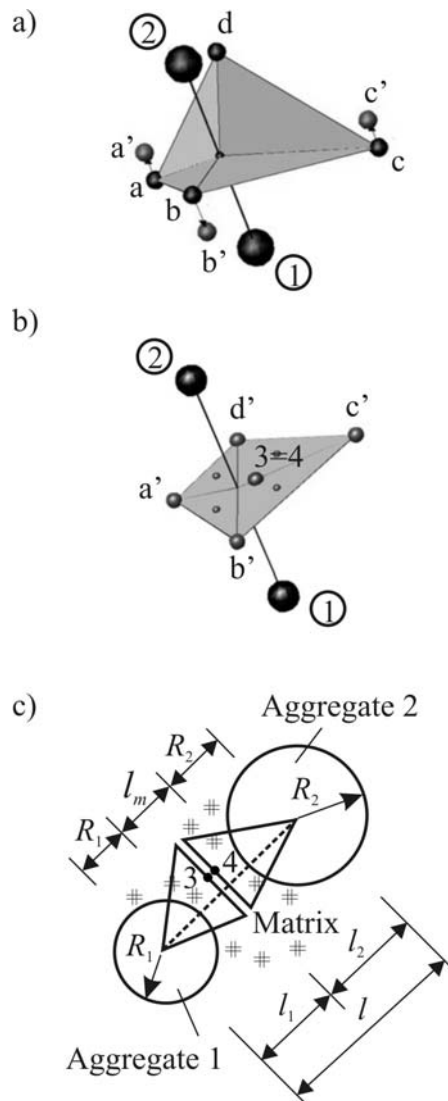


Figure 1. a) Contact area between the aggregates 1 and 2. b) Projected contact area showing the assumed contact point 3=4. c) Definition of the lengths  $l_1$ ,  $l_2$ , and  $l_m$ .

7. the strains are defined by smearing over the length of each lattice element the relative displacements at the contact point which, in turn, are computed by assuming a rigid relative motion of the two adjacent particles;
8. the tensile and shear behaviors of the connecting struts are sensitive to the confinement in directions orthogonal to the strut;
9. the shear response of the lattice element shows friction and cohesion.

The contact area between two adjacent aggregates (area  $abcd$  in Figure 1a for the

aggregates 1 and 2) is, in general, not planar and not orthogonal to the connection. For sake of simplicity, the constitutive law is imposed on the projection of this area on a plane orthogonal to the connection (area  $\underline{a'b'c'd'}$  in Figure 1b). The contact point (point 3=4 in Figure 1b), considered as the center of mass of the projected area, is not located along the connection (as in the previous versions of the model).

The normal and shear strains are defined, incrementally, as follows

$$d\varepsilon_N = \frac{u_2 - u_1 + (\phi_2 - \phi_1)e_z + (-\theta_2 + \theta_1)e_y}{l} \quad (1)$$

$$d\varepsilon_M = \frac{v_2 - v_1 - \theta_2 l_2 - \theta_1 l_1 - \psi_2 e_z + \psi_1 e_y}{l} \quad (2)$$

$$d\varepsilon_L = \frac{w_2 - w_1 + \phi_2 l_2 + \phi_1 l_1 + \psi_2 e_y - \psi_1 e_z}{l} \quad (3)$$

Here  $u_1, u_2$  are the displacements of the two connected aggregates in the direction of the line connecting their centers,  $v_1, v_2, w_1$  and  $w_2$  are the transversal displacements and  $\theta_1, \theta_2, \phi_1, \phi_2, \psi_1$  and  $\psi_2$  are the spatial rotations of the aggregates in a local system of reference. The lengths  $l_1 = l_m/2 + R_1$  and  $l_2 = l_m/2 + R_2$  define the position of the contact point,  $R_1, R_2$  are the radii of the aggregates 1 and 2, respectively and  $l_m$  is the thickness of the matrix along the connection line (Fig. 1c). The symbols  $e_y$  and  $e_z$  represent the eccentricity of the contact point respect to the connection axis. All the strain components are considered as uniformly distributed over the length  $l$  of the strut. The stress-strain relations are given as

$$\sigma_N = \frac{\sigma}{\varepsilon} \varepsilon_N; \quad \sigma_M = \alpha \frac{\sigma}{\varepsilon} \varepsilon_M; \quad \sigma_L = \alpha \frac{\sigma}{\varepsilon} \varepsilon_L \quad (3)$$

in which  $\sigma$  (*effective stress*) is assumed to be a function of  $\varepsilon = (\varepsilon_N^2 + \alpha \varepsilon_T^2)^{1/2}$  (*effective strain*) and  $\omega = \arctan[\varepsilon_N / (\alpha^{1/2} \varepsilon_T)]$  (*coupling strain*) where  $\varepsilon_T = (\varepsilon_M^2 + \varepsilon_L^2)^{1/2}$  is the *total shear strain* and  $\alpha$  is a constant material parameter which represents the ratio between shear and normal stiffnesses of the connecting strut.

The elastic behavior is represented by the incremental relation  $d\sigma = E d\varepsilon$ , where the normal elastic modulus  $E$  is obtained by coupling in series the effect of the aggregates and the embedding matrix:  $E = l / (l_m/E_m + l_a/E_a)$  and  $l_a = R_1 + R_2, l_m = l - l_a$ .

The nonlinear behavior is simulated by using the concept of stress-strain boundary (strain-dependent yield limit also used for the microplane model formulation, Bažant et al. 1996, Bažant et al. 2000, Bažant & Caner 2002) which is imposed by the inequality  $0 \leq \sigma \leq \sigma_b$  where

$$\sigma_b = \sigma_0(\omega) \exp\left(K(\omega) \frac{\langle \varepsilon - \varepsilon_0(\omega) \rangle}{\sigma_0(\omega)}\right) \quad (4)$$

Here  $\sigma_0(\omega)$  is the effective strength,  $\varepsilon_0(\omega) = \sigma_0(\omega)/E$  is the elastic strain limit, and  $K(\omega)$  governs the effective stress evolution in the non linear range.  $K(\omega)$  is negative (softening behavior) for tension, shear with tension, and shear with low compression, but it is positive (hardening behavior) for compression and shear with high compression. The constitutive relation is assumed to depend on the confinement strain,  $\lambda$ , transversal to the connection which is obtained by projecting orthogonally to the connection the average of the strain tensors computed in the adjacent tetrahedra assuming a linear distribution of displacements and neglecting the effect of particle rotations. The confinement dependence is introduced in the formulation by defining the initial post peak slope  $K_t$  of the pure mesolevel tensile behavior as it follows

$$K_t = \frac{2E_N}{l_{cr} / l - 1} f(\lambda); \quad f(\lambda) = \frac{1}{1 + \langle -\lambda / \lambda_0 \rangle} \quad (5)$$

where  $l_{cr} = 2E_N G_t / \sigma_t^2$ ;  $E_N$  is the normal stiffness of the connection,  $\sigma_t$  is the tensile mesostrength. The characteristic strain parameter  $\lambda_0$  governs the sensitivity to confining strain. The details of the formulation appear in Cusatis (2001), Cusatis et al. (2003a) and in Cusatis (2003).

The present model can realistically simulate, by using the same mesolevel material parameters, tensile fracturing, cohesive fracture and size effect (Cusatis 2001, Pisanu & Pedroni 2003, Cusatis et al. 2003b), compression-shear behavior with softening at zero or mild confinement (Cusatis 2001, Cusatis 2003b and Polli 2003), and response at high confined compression at which there is only hardening (Cusatis 2001). The model has been also used to simulate the performance of headed stud anchors with good agreement with the experimental evidences (Rota & Rosson 2002, Cusatis et al. 2003c)

### 3 NUMERICAL SIMULATION OF MODE I FRACTURE PROPAGATION

Let us now simulate the response of single notched specimens under tensile loading. The simulated specimens are squares of  $100 \times 100$  mm<sup>2</sup> and thickness equal to 50 mm. The notch is 20 mm long and 3 mm wide. The load is applied under displacement control allowing free rotations of the loading platens. Twelve specimens are generated randomly, considering the following granulometric

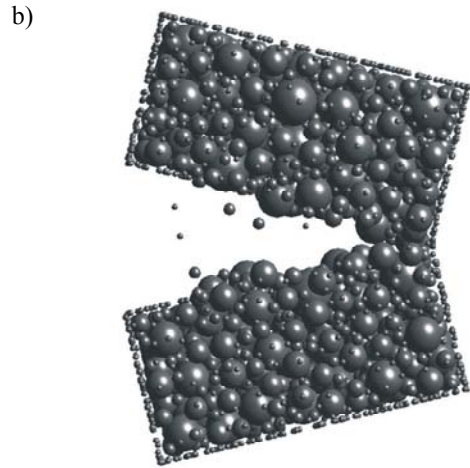
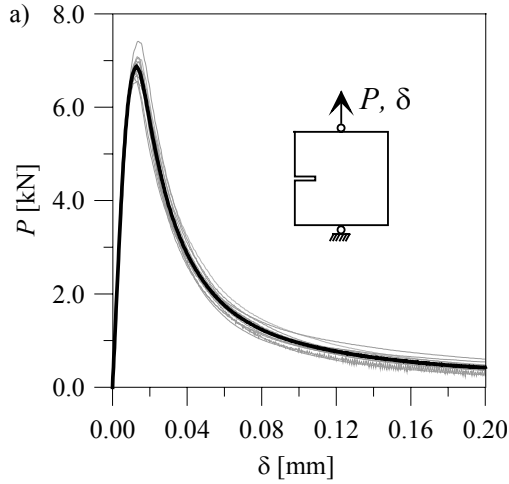


Figure 2. a) Numerical load-displacement curves obtained by the CSL model. b) Amplified (100 times) deformed shape

distributions: 5.4%, 17.4%, 16.7%, 8.4%, 7% and 4% (mass fractions) of aggregates with characteristic sizes of 16 mm, 12.5 mm, 9.5 mm, 8 mm, 6.3 mm and 4.0 mm, respectively.

The reference material properties are: cement content  $c=300 \text{ kg/m}^3$ , water-cement ratio  $w/c=0.6$ , aggregate-cement ratio  $a/c=6.4$ . The parameters of the mesolevel constitutive law, used for the numerical calculations, are the following:  $\alpha=0.25$ , normal elastic modulus of cement  $E_c=11250 \text{ MPa}$ , normal elastic modulus of aggregate  $E_a=6 E_c$ , tensile meso-strength (strength at the meso-level of microstructure)  $\sigma_t=2.4 \text{ Mpa}$ , fracture energy at meso-level (without confining effect)  $G_f=0.03 \text{ N/mm}$ ; meso-cohesion  $\sigma_s=3\sigma_t$ , compressive meso-strength  $\sigma_c=16\sigma_t$ , hardening parameter at meso-level  $K_c=0.26E_c$ , shape parameter of compression

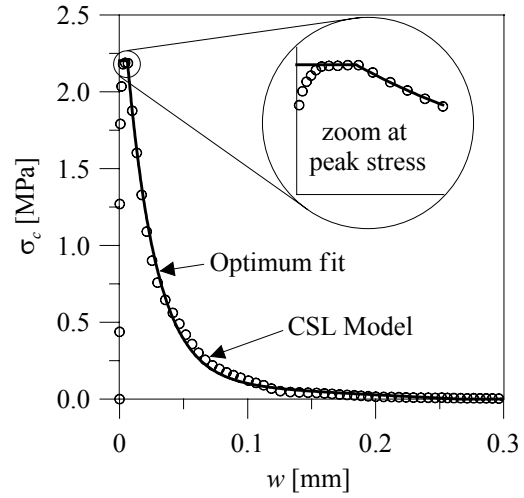


Figure 3. Obtained macroscopic cohesive crack law and its optimum fit.

cap  $\beta=1$ ; asymptotic slope of the frictional hyperbola  $\mu=0.2$ ,  $n_r=n_c=2$  (see Cusatis et al. 2003b); and characteristic strain defining the confinement effect  $\lambda_0=1 \times 10^{-3}$  (Cusatis 2003, Polli 2003). Figure 2a shows the numerical results in terms of load-displacement ( $P$ - $\delta$ ) curves. The gray lines are the response of the twelve specimens and the black line represents the averaged response. In Figure 2b shows the amplified (100 times) deformed shape at the end of the test of one of the simulated specimens. The fracture initiates exactly at the notch tip and propagates almost straight. Its irregular surface is basically due to the aggregate pieces located across the specimen ligament.

#### 4 MACROSCOPIC COHESIVE CRACK MODEL IDENTIFICATION

In this section the meso-level response of the concrete specimens simulated in Section 3 is analyzed in order to identify an equivalent macroscopic cohesive crack law (cohesive stress vs. crack opening displacement).

To this end, the ligament of the specimens is subdivided into segments (of length  $h \approx 3.0 \text{ mm}$ ). For each segment and loading step, the macroscopic cohesive stress (constant over the segment),  $\sigma_c$ , in the direction of the applied load and the dissipated energy per unit ligament area,  $G_d$ , are computed by averaging the mesolevel response.

Since the macro-crack opening displacement,  $w$ , is the work-conjugate quantity of the cohesive stress, the latter may be computed by integrating the differential equation  $dG_d = \sigma_c dw$ . We can write

$$w(G_d) = \int \frac{dG_d}{\sigma_c(G_d)} \quad (6)$$

The functions  $\sigma_c(G_d)$  and  $w(G_d)$  give a parametric representation of the crack cohesive law. Figure 3 shows a generic cohesive law obtained at a certain location along the ligament.

In the first part of the curve the stress increases with no opening of the crack (and no energy dissipation as well) describing the elastic regime. At a certain stress threshold inelastic phenomena occur and the crack opening starts to increase. During this stage the stress still increases following a hardening behavior (zoom in Figure 3). It must be stressed that this result is not due to the mesolevel constitutive law, which is always softening for tensile dominant stress state, but it comes from the stress redistribution occurring in the mesostructure. In this phase the dissipated energy is mainly due to the initiation and growth of meso-cracks and it is not associated to a real macro-crack. The initiation of a real macro-crack occurs when hardening behavior reverses into softening and the stress decreases for increasing crack opening displacement (and dissipated energy). The shape of the post-peak branch of the curve is nearly exponential right after the peak but it shows a tail which is basically linear. The optimum fit, shown in Figure 3, has been obtained by assuming a cohesive crack law with an initial plateau followed by a smooth curve consisting of the sum of a straight line and an exponential function. The equation of such a curve is  $f(w) = f'_i$  for  $w < w_0$ ,  $f(w) = 0$  for  $w > w_u$  and

$$f(w) = f'_i \left[ c_1 - c_2 \frac{w - w_0}{w_{ch}} + (1 - c_1) e^{-c_3 \frac{w - w_0}{w_{ch}}} \right] \quad (7)$$

for  $w_0 \leq w \leq w_u$ , being  $w_u$  the value of the crack opening displacement for which the function in Equation 7 goes to zero.

The optimization of the parameters has been done, for each segment of the ligament by using the Levenberg-Marquardt method.

It must be noticed that from a rigorous point of view, the energy dissipation related to the first non-softening part of the cohesive law should be taken into account by assuming a plastic hardening behavior of the stress-strain relationship of the intact concrete instead of introducing it directly in the cohesive formulation. This was also demonstrated experimentally by Cedolin et al. (1987).

Regarding the tail of the obtained cohesive curve it is worth pointing out that the linear evolution is

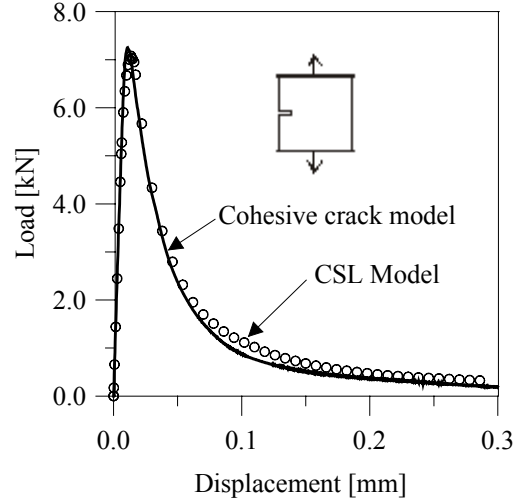


Figure 4. Comparison between the load-displacement curve obtained by the CSL model and the equivalent cohesive crack model.

an effect of the frictional interaction between the aggregates which is captured by the model even if the local (meso-level) constitutive relation is purely exponential for tension and shear.

In order to validate this procedure a cohesive crack simulation, assuming the macroscopic cohesive law identified at each discrete point along the ligament from the lattice analysis, has been performed. Figure 4 shows the comparison between the lattice and cohesive crack simulations, which agree quite well.

The previous procedure has been repeated for each of the twelve specimens. The results, in terms of the fracture energies (total fracture energy and initial fracture energy) and the tensile strength, are shown in Figures 5 and 6, respectively. The solid curves represent the mean value at each ligament location, the error bar is the mean plus-minus the standard deviation and the dashed line is average of all mean values over the ligament.

The obtained mean curves appear quite irregular even if they come from the average of twelve specimens. The reason is that, probably, the ligament size (80 mm) of the assumed specimen geometry is too small compared to the maximum aggregate size (16 mm). Nevertheless some interesting trends can be observed. The total fracture energy  $G_F$  (top of Fig. 5) first increases, moving from the notch tip to the interior of the specimen and afterwards it decreases while approaching the opposite boundary. This result is in agreement with some experimental findings (e.g. Brameshuber et al. 1990 and Hu & Wittmann 1992).

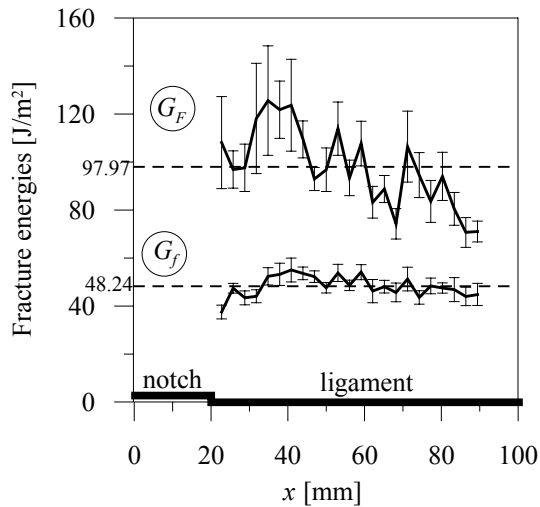


Figure 5. Macroscopic fracture energy profiles along the ligament

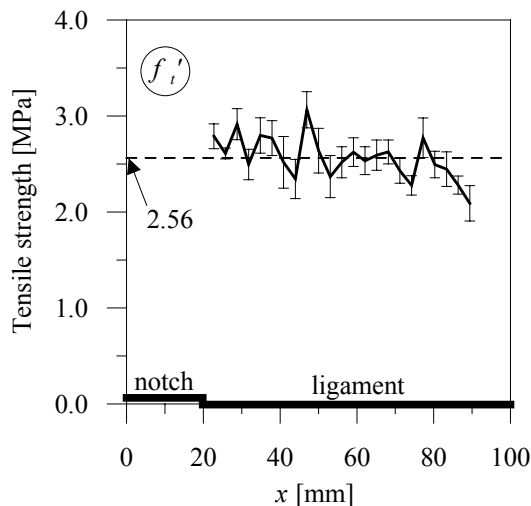


Figure 6. Macroscopic tensile strength profile along the ligament

This boundary effects is less pronounced for the initial fracture energy  $G_f$  (bottom of Fig. 5). In particular the effect of the opposite edge seems to be negligible. Moreover, the standard deviation of the initial fracture energy  $G_f$  is significantly smaller than the standard deviation of the total fracture energy  $G_F$ , corroborating the results obtained by Bažant & Becq-Giraudon (2001). The trend of the tensile strength (Fig. 6) seems not to be influenced by the boundary but the scatter of the results is such that no clear conclusions can be drawn. However it is interesting to notice that the mean value over the ligament (2.56 Mpa) is higher than

the tensile strength computed by direct tensile test which for the assumed meso-level material parameters is 2.34 MPa (Polli 2003). Also this result is in full agreement with the findings of Cedolin et al. (1987).

We must notice that in the previous discussion the cohesive crack model is considered as a *local property* (rather than a property of the material representative volume) whose randomness, due to the meso-structure heterogeneity, is filtered out by averaging, at each material point, the responses obtained from various specimens with different meso-structures. This approach differs from the usual definitions adopted for the macroscopic properties of random composites, in which the mean behavior is captured by averaging the response over the representative volume. This is however meaningful if the size of the specimen is several times the dimension of the representative volume. Otherwise the averaging procedure would also include the effects of the boundary conditions, leading to erroneous conclusions. Unfortunately this is quite often the situation observed for the concrete specimens used in the experiments and analyzed in this paper. On the other hand it is not clear at the moment if the *local* approach really leads to actual macroscopic material properties and further investigations are surely needed.

## 5 ACKNOWLEDGMENT

The help of A. Carlucci for the cohesive crack simulations is gratefully acknowledged.

## 6 REFERENCES

- Bažant, Z.P. & Caner, F. 2002. *Microplane model M5 with kinematic and static constraints for concrete fracture and anelasticity*. Structural Engineering Report No. 02-12/C699m, Northwestern University, Evanston, Illinois;
- Bažant, Z. P., Caner, F., Carol, I., Adley, M. & Akers, S.A. 2000. Microplane Model M4 for Concrete. I: formulation with work-conjugate deviatoric stress. *Journal of Engineering Mechanics*, ASCE 126, No. 9: 944-953.
- Bažant, Z.P. & Becq-Giraudon, E. 2001. Estimation of fracture energy from basic characteristics of concrete. *Fracture Mechanics of Concrete*, FraMCoS-4: 491-495.
- Bažant, Z. P., Tabarra, M. R., Kazemi, T. & Pijaudier-Cabot, G. 1990. Random particle model for fracture of aggregate or fiber composites. *Journal of Engineering Mechanics*, ASCE, 116(8): 1686-1705.
- Bažant, Z.P., Xiang, Y. & Prat, P.C. 1996. Microplane model for concrete. I. Stress-strain boundaries and finite strain. *Journal of Engineering Mechanics*, ASCE, 122(3): 245-254.
- Bolander, J. E., Hong, G. S. & Yoshitake, K. 2000. Structural concrete analysis using rigid-body-spring networks. *Journal of Computer Aided Civil and Infrastructure Engineering*, 15: 120-133.

- Bolander, J. E. & Saito, S. 1998. Fracture analysis using spring network with random geometry. *Engineering Fracture Mechanics*, 61(5-6): 569-591.
- Bramshuber, W. & Hilsdorf, H. K. 1990. Influence of ligament length and stress state on fracture energy of concrete. *Engineering Fracture Mechanics*. 35(1-3): 95-106.
- Carol, I., López, C. M. & Roa, O. 2001. Micromechanical analysis of quasi-brittle materials using fracture-based interface elements. *International Journal for Numerical Method in Engineering*, 52: 193-215.
- Cedolin, L., Dei Poli, S. & Iori, I. 1987. Tensile behavior of concrete. *Journal of Engineering Mechanics*, ASCE, 113(3): 431-449
- Cusatis, G. 2001. *Tridimensional random particle model for concrete*, PhD Thesis. Department of Structural Engineering, Politecnico di Milano, Milan, Italy.
- Cusatis G. 2003. *Private communication to Z.P. Bažant*. Sept. 22.
- Cusatis G., Bažant, Z.P. & Cedolin L. 2003a. Confinement-shear lattice model for concrete damage in tension and compression: I. Theory. *Journal of Engineering Mechanics*, ASCE, 129(12): 1439-1448.
- Cusatis G., Bažant, Z.P. & Cedolin L. 2003b. Confinement-shear lattice model for concrete damage in tension and compression: II: Numerical implementation and Validation. *Journal of Engineering Mechanics*, ASCE 129(12): 1449-1458.
- Cusatis, G., Di Luzio, G. & Rota, G. 2003c. Simulation of Headed Anchor Failure. *EURO-C 2003. Computational Modelling of Concrete Structures*: 683-688, St. Johann im Pongau, Austria. March 17-20, 2003.
- Guinea, G.V., Planas, J. & Elices, J. 1992. Measurement of the fracture energy using three-point bend tests: Part 3-Influence of cutting the  $P-\delta$  tail. *Materials and Structures*, 25: 212-218
- Hillerborg, A., Modéer, M. & Petersson, P.E. 1976. Analysis of crack formation and crack growth in concrete by means of fracture mechanics and finite elements. *Cement and Concrete Research*, 6: 773-782.
- Hu, X.Z & Wittmann, F.H. 1992. Fracture energy and fracture process zone. *Materials and Structures*, 25: 319-326
- Lilliu, G. & van Mier J. G. M. 2003. 3D lattice type fracture model for concrete. *Engineering Fracture Mechanics*, 70: 927-941.
- López, C. M., Carol, I. & Murcia, J. (2001). Mesostructural modeling of basic creep at various stress levels. *Sixth international conference CONCREEP-6@MIT*: 101-106.
- Pisanu, A. & Pedroni, L. 2003. *Numerical simulation of concrete fracturing behavior: size effect and boundary condition effect* (in Italian). Master Thesis. Department of Structural Engineering, Politecnico di Milano, Milan, Italy.
- Polli, M. 2003. *Meso-structural modeling for the simulation of the concrete fracturing behavior* (in Italian). Master Thesis. Department of Structural Engineering, Politecnico di Milano, Milan, Italy.
- Roelfstra, P. E., Sadouki, H. & Wittmann, F. H. 1985. Le béton numérique. *Materials and Structures -RILEM*, 18: 327--335.
- Rota, G. & Rosson, M. 2002. *Numerical simulation of headed anchors in R/C structures* (in Italian). Master Thesis. Department of Structural Engineering, Politecnico di Milano, Milan, Italy.
- Schlagen, E. & van Mier, J. G. M. (1992). Shear fracture in cementitious composites. Part II: Numerical simulations. *Fracture mechanics of concrete structures*, FraMCoS-1: 671-676.